Dissipation effect in the double-well Bose-Einstein Condensate

Hanlei Zheng, Yajiang Hao and Qiang Gu*
Department of Physics, University of Science and Technology Beijing, Beijing 100083, China
(Dated: November 22, 2012)

Dynamics of the double-well Bose-Einstein condensate subject to energy dissipation is studied by solving a reduced one-dimensional time-dependent Gross-Pitaevskii equation numerically. We first reproduce the phase space diagram of the system without dissipation systematically, and then calculate evolutionary trajectories of dissipated systems. It is clearly shown that the dissipation can drive the system to evolve gradually from the π-mode quantum macroscopic self-trapping state, a state with relatively higher energy, to the lowest energy stationary state in which particles distribute equally in the two wells. The average phase and phase distribution in each well are discussed as well. We show that the phase distribution varies slowly in each well but may exhibit abrupt changes near the barrier. This sudden change occurs at the minimum position in particle density profile. We also note that the average phase in each well varies much faster with time than the phase difference between two wells.

PACS numbers: 03.75.Lm, 05.30.Jp, 05.30.Rt

I. INTRODUCTION

The experimental realization of atomic Bose-Einstein condensation has stimulated great interest in quantum nature of the condensate of weakly interacting bosons. Since the condensate is in the macroscopic quantum state, a variety of quantum phenomena show up when two condensates are linked. If the two condensates are separated by a barrier through which atoms can tunnel, a bosonic Josephson junction (BJJ) is built and allows for the detection of Josephson-like current-phase effects, analogous to two weakly coupled superconductors. This phenomenon was initially predicted by Javanainen [1] and was further demonstrated by a number of researchers using various techniques [2–12]. In addition, the dc and ac Josephson effects [2–5] as well as the Shapiro effect [5] in BJJs have been discussed.

Furthermore, many theoretical works reveal that the BJJ can exhibit new phenomena that are not accessible with superconductor Josephson junctions (SJJs). The mean-field theory based on two-mode approximation predicted the π-phase oscillations and macroscopic quantum self-trapping (MQST) [4, 5]. The MQST is a fascinating nonlinear phenomenon which arises from interactions between atoms. Quantum corrections to the mean-field results were also intensively discussed [6–12], providing a number of fascinating observations, such as collapse and revival of quantum oscillations [6], occupancy of phase-squeezing state [7], disappearance of coherence [8, 9], and destruction of the self-trapped state [10].

In above studies the double-well condensate is treated as an isolated system, but actually it is coupled to certain thermal cloud and subject to environment distortions [13–16]. Ruostekoski and Walls studied the energy dissipation in BJJs via stochastic simulations in a two-mode approximation and showed that the MQST decays away [13]. Wimberger *et al.* discussed dynamics of the double-well condensate subject to phase noise and particle loss and indicated that coherence might be increased to a maximum for proper dissipation [15]. They argued that this phenomenon can be understood as a stochastic resonance of the many-particle system.

On experimental side, the MIT team carried out the first double-well experiment and gained interference patterns proving the coherence of BEC [17]. In 2005, Albiez *et al.* reported the direct observation of the quantum tunneling and macroscopic self-trapping for a single BJJ [18]. They measured the density distribution *in situ* and deduced the relative phase versus time from interference fringes. A summary of the observed static, thermal and dynamical properties was given in Ref. [19]. After that the dc Josephson effect was also achieved [20]. A classical bifurcation was studied at the transition from the Rabi to Josephson oscillations [21].

In this paper, we concentrate on dynamical behaviors of the double-well condensate subject to energy dissipation based on the time-dependent Gross-Pitaevskii (TDGP) equation. The TDGP equation provides a very good description of dynamical evolution of trapped dilute Bose gases at temperature far below the critical temperature [22, 23]. The two-mode approximation for the BJJ is an extremely simplified version of the TDGP equation. Although it can give a qualitatively description of the BJJ system [2, 4, 13, 15], the two-mode model ignores the spatial distribution of the density and phase. Whereas, these information could be obtained from the Gross-Pitaevskii (GP) equation [22].

This paper is organized as follows. In Sect. II, the TDGP equation is introduced to describe the double-well condensate, where a phenomenological term is added to account for the energy dissipation. In Sect. III, we reproduce numerically the phase space diagram of the double-well condensate without dissipation, and make a comparison with the two-mode model results. Sect. IV discusses

*Email: qgu@ustb.edu.cn

the dissipation effect. A summary is given in the last section.

II. THE MODEL

A. Time-dependent Gross-Pitaevskii (TDGP) equation

The general formalism of three-dimensional (3D) time-dependent Gross-Pitaevskii equation for dilute Bose gases trapped in the double-well potential at zero temperature reads

$$\imath\hbar\frac{\partial\psi(\mathbf{r};t)}{\partial t}=\left[-\frac{\hbar^2}{2m}\nabla^2+V(\mathbf{r})+gN|\psi(\mathbf{r};t)|^2\right]\psi(\mathbf{r};t), \quad (1)$$

where $\psi(\mathbf{r};t)$ is the macroscopic wave function at position $\mathbf{r}$ and time t, m is the mass of an atom, $g=4\pi\hbar^2a/m$ is the nonlinear constant with a the s-wave scattering length, and N is the total atom number. The double-well potential $V(\mathbf{r})$ is given by $V(\mathbf{r})=\frac{m}{2}(\omega_x^2r_x^2+\omega_y^2r_y^2+\omega_z^2r_z^2)+V_{\rm b}\cos^2(\pi r_z/q_0)$ [23], where the first term describes a harmonic trap with trap frequencies $\omega_{x,y,z}$, and the second denotes the barrier potential. Hereinafter we set $\omega_x=\omega_y=\omega_\perp\gg\omega_z$.

Assuming that the dynamical evolution mostly takes place in the direction containing the barrier, the 3D GP equation can be reduced to a simpler one-dimensional (1D) form [24]. Such reduction is reasonable in the case of a strong trapping in the other two spatial directions, say, in the x-y plane. Then the 1D GP equation in z axis only with dimensionless quantities is given by [25]

$$\imath\frac{\partial\bar{\psi}(z;\tau)}{\partial\tau}=\left[-\frac{\partial^2}{\partial z^2}+v_{1D}(z)+\frac{g_{1D}\beta}{\pi}|\bar{\psi}(z;\tau)|^2\right]\bar{\psi}(z;\tau), \quad (2)$$

where $z=r_z/l_z$, $\tau=t\omega_z/2$ and $\beta=\omega_\perp/\omega_z$. The dimensionless parameters are scaled by the characteristic length $l_z=\sqrt{\hbar/(m\omega_z)}$ and energy $\hbar\omega_z$ correspondingly. The 1D potential is reduced to $v_{1D}(z)=z^2+2v_{\rm b}\cos^2(\pi z/q_0')$, with $v_{\rm b}=V_{\rm b}/(\hbar\omega_z)$ and $q_0'=q_0/l_z$. $g_{1D}=gNm/(l_z\hbar^2)$ is the dimensionless interaction parameter. This reduction greatly simplifies the computation. The wave function $\bar{\psi}(z;\tau)$ satisfies the normalization condition,

$$\int_{-\infty}^{\infty}{\rm d}z|\bar{\psi}(z;\tau)|^2=1. \quad (3)$$

The reduced TDGP equation can be solved by a commonly accepted numerical algorithm called Split-Step Crank-Nicolson scheme with space and time both discretized [25]. In numerical calculation, t is measured in $\omega_z/2$. If $\omega_z=2\pi\times10Hz$, $\tau=1$ corresponds to $t=31.8ms$.

B. The TDGP equation with dissipation

Choi *et al.* has described a phenomenological damping theory based on the TDGP equation [26]. A phenomenological parameter γ is introduced in the GP equation to account for the dissipation rate. The reformed TDGP equation is written as

$$(\imath-\gamma)\frac{\partial\bar{\psi}(z;\tau)}{\partial\tau}=\left[-\frac{\partial^2}{\partial z^2}+v_{1D}(z)+\frac{g_{1D}\beta}{\pi}|\bar{\psi}(z;\tau)|^2\right]\bar{\psi}(z;\tau). \quad (4)$$

The phenomenological parameter γ characterizes the strength of dissipation and its value may be determined experimentally. Choi *et al.* got that $\gamma=0.03$ by fitting theoretical results with the MIT experiments dates. This approach is comparable to the generalized finite-temperature GP equation derived by Zaremba, Nikuni and Griffin [27],

$$\imath\hbar\frac{\partial\Psi(\mathbf{r};t)}{\partial t}=[-\frac{\hbar^2}{2m}\nabla^2+V(\mathbf{r})+gn+2g\tilde{n}-i\Gamma]\Psi(\mathbf{r};t), \quad (5)$$

where $n(\mathbf{r};t)=|\Psi(\mathbf{r};t)|^2$ is the condensate density and $\tilde{n}(\mathbf{r};t)$ is the noncondensate density. Dissipation arises from collisions between the condensate and noncondensate atoms.

Ueda *et al.* have successfully employed this phenomenological approach to study the detailed dynamics of a sudden rotated BEC in a trap with $\gamma=0.03$ and figured out the vortex lattice formation process [28]. This approach is also used to study the Bose-Einstein droplet in free space [29], vortex formation in Bose-Einstein condensates in a rotating double-well potential [30] and the decay of dark solitons in harmonically trapped, partially condensed Bose gases in the presence of phase fluctuations or dynamical noise [31]. These works prove that the phenomenological damping description does indeed provide an efficient numerical tool for the research of BECs in an open system.

C. The phase difference and phase distribution

As discussed in the introduction, we consider two Bose-Einstein condensates with repulsive interaction in a Quasi-1D symmetric double-well potential, which could be experimentally realized by splitting a single well into two parts: one cigar-shaped atomic cloud is cut into two separated aligned cigars. It is necessary to construct an approximate initial state of the double-well condensate at first. We set ϕ_L for the wave packet mostly localized in the left well and ϕ_R the right one. The original trial wave function is forged as a superposition of ϕ_L and ϕ_R,

$$\bar{\psi}(z;\tau)=\psi_L(\tau)\phi_L(z)+\psi_R(\tau)\phi_R(z), \quad (6)$$

where $\psi_{L(R)}(\tau)=\sqrt{n_{L(R)}(\tau)}{\rm e}^{i\theta_{L(R)}(\tau)}$. $n_{L(R)}(\tau)$ corresponds to fraction of atoms on the left (right) side of the trap, and therefor $n_L(\tau)+n_R(\tau)=1$. They are constructed as linear combinations of the two lowest stationary modes of the 1D GP equation, the symmetric

ϕ_+ and antisymmetric ϕ_-. $\phi_L(z) = \frac{\phi_+(z)+\phi_-(z)}{2}$ and $\phi_R(z) = \frac{\phi_+(z)-\phi_-(z)}{2}$. $\phi_+(z)$ and $\phi_-(z)$ can be obtained by the method of imaginary-time propagation where the time variable τ in Eq. (2) is replaced with an imaginary time.

The initial state with a given initial imbalance at $t = 0$ is constructed as follow

$$\bar{\psi}(z;0) = \mathrm{e}^{i\Delta\theta(0)}\sqrt{n_L(0)}\psi_L(z) + \sqrt{n_R(0)}\psi_R(z), \quad (7)$$

where $\Delta n(0) = n_L(0) - n_R(0)$ and $\Delta\theta(0)$ represent the initial population imbalance and phase difference in the double-well. The dynamical evolution is calculated by solving Eq. (2) through real-time propagation method.

Once $\bar{\psi}(z;\tau)$ is obtained, the atom fraction in the left and right well could be computed by $n_L(\tau) = \int_{-\infty}^{0} \mathrm{d}z|\bar{\psi}(z;\tau)|^2$ and $n_R(\tau) = \int_0^{\infty} \mathrm{d}z|\bar{\psi}(z;\tau)|^2$. The population imbalance is $\Delta n(\tau) = n_L(\tau) - n_R(\tau)$. The phase of condensates in the left well is defined as

$$\theta_L(\tau) = \arctan\frac{\int_{-\infty}^{0} \mathrm{d}z\mathrm{Im}[\bar{\psi}(z;\tau)]\rho(z;\tau)}{\int_{-\infty}^{0} \mathrm{d}z\mathrm{Re}[\bar{\psi}(z;\tau)]\rho(z;\tau)}, \quad (8)$$

and in the right well

$$\theta_R(\tau) = \arctan\frac{\int_{0}^{\infty} \mathrm{d}z\mathrm{Im}[\bar{\psi}(z;\tau)]\rho(z;\tau)}{\int_{0}^{\infty} \mathrm{d}z\mathrm{Re}[\bar{\psi}(z;\tau)]\rho(z;\tau)}, \quad (9)$$

where $\rho(z;\tau) = \bar{\psi}^*(z;\tau)\bar{\psi}(z;\tau)$. The phase difference is $\Delta\theta(\tau) = \theta_L(\tau) - \theta_R(\tau)$.

Moreover, we could get the phase at a certain point at a certain time which is different from that of the two-mode model.

$$\theta(z;\tau) = \arctan\frac{\mathrm{Im}\left[\bar{\psi}(z;\tau)\right]}{\mathrm{Re}\left[\bar{\psi}(z;\tau)\right]}. \quad (10)$$

III. THE PHASE SPACE DIAGRAM

In following calculations, we set $\beta = 10$, $v_b = 5$ and the dimensionless trap geometry are chosen as $v_{1D}(z) = z^2 + 10\cos^2(\pi z/5.2)$, where $q_0' = 5.2$ is calculated from the experiment parameter in Ref. [18], $q_0 \sim 5\mu m$. However, the dimensionless interacting strength g_{1D} is a tunable parameter. It varies with particle number of the system, N. The time step is $\delta\tau = 0.001$ and space step $\delta z = 0.01$ in the calculation.

The evolution of the population imbalance Δn and the phase difference $\Delta\theta$ can be calculated from Eq. (2). Figure 1 shows the obtained results for $g_{1D} = 0.01$, with the initial states being ($\Delta n = 0.9$ $\Delta\theta = 0$), (0.9, π) and (0.5, π), respectively. The solid lines in Fig. 1(a) and 1(b) depict evolutions from the state ($\Delta n = 0.9$ $\Delta\theta = 0$). Both the population imbalance and the phase difference oscillate around zero ($\Delta n = 0$ and $\Delta\theta = 0$) with time. This denotes the Josephson oscillation mode. In the other two cases, Δn is always positive which means

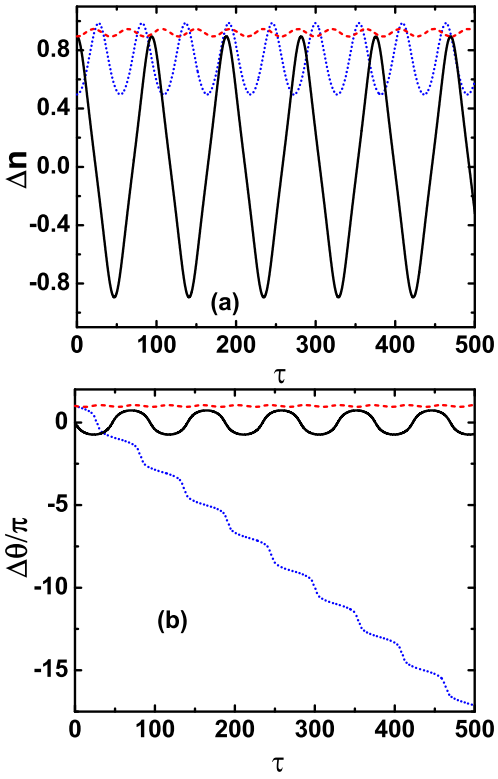

FIG. 1: (Color online) The Δn-τ plot (a) and $\Delta\theta$-τ plot (b). The solid lines, short-dashed lines, and short-dotted lines represent the evolutions from the initial state ($\Delta n = 0.9$ $\Delta\theta = 0$), ($\Delta n = 0.9$ $\Delta\theta = \pi$) and ($\Delta n = 0.5$ $\Delta\theta = \pi$), respectively.

that the particle number in the left well is always larger that in the right well. This is referred to as the so-called macroscopic quantum self-trapping phenomenon [4]. As shown in Fig. 1(b), the short dashed-line oscillates around $\Delta\theta = \pi$ while the short-dotted line indicates that the phase changes monotonously with time. Such tendency characterize the difference between the π-mode MQST and running phase MQST.

By combining evolutions of Δn and $\Delta\theta$, the Δn-$\Delta\theta$ phase space diagram can be constructed. Fig. 2(a) displays the three kinds of evolutions discussed above. (i) The Josephson oscillation mode characterized by the time-average particle imbalance $\langle\Delta n\rangle_\tau = 0$ is represented by closed orbits around $\Delta\theta = 0$ (or $\Delta\theta = 2k\pi$ where k is an integer). (ii) The π-mode MQST is represented by the closed orbits around $\Delta\theta = \pi$ (or $\Delta\theta = (2k \pm 1)\pi$). (iii) The open orbits between the above two types of closed orbits refer to the running-phase MQST. The particle imbalance $\langle\Delta n\rangle_\tau \neq 0$ for both the two MQST modes.

The Δn-$\Delta\theta$ phase space diagram has been produced previously based on the two-mode model [4]. As Ref. [4] suggested, each orbit denotes a constant energy contour line. The π-mode has relative high energy. The energy maxima lie at the center of the π-mode closed orbits and there are two maxima symmetrically located on both sides of $\Delta n = 0$ axis. On the contrary, the Joseph-

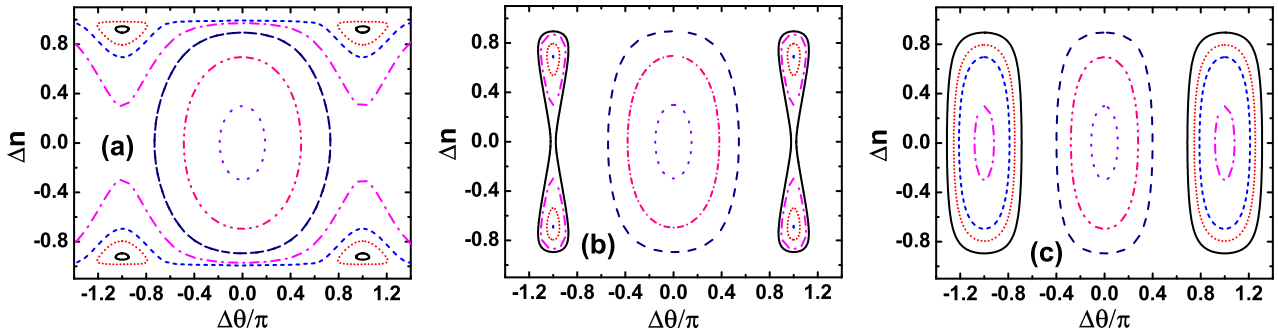

FIG. 2: (Color online) The Δn-$\Delta\theta$ phase space diagram for different interaction strengths. (a) $g_{1D} = 0.01$, (b) $g_{1D} = 0.005$, (c) $g_{1D} = 0.001$. The orbits are presented by constant energy lines.

son oscillation mode has smaller energy and the energy minimum is located at the points ($\Delta n = 0$, $\Delta\theta = 2k\pi$).

Nevertheless, it is suggested that the two-mode model has to be improved to agree with experimental observations [18]. Meanwhile, it is shown that the TDGP equation provides more accurate simulation of dynamical evolution of the double-well condensate than the two-mode model [22, 23]. Unlike the two-mode model which ignores the spatial information, the TDGP equation deals with the spatial distribution of density and phase, thus it achieves quantitative accuracy of dynamics of the condensate. The present study produces the Δn-$\Delta\theta$ phase space diagram systematically within the framework of TDGP equation.

MQST is a kind of nonlinear effect which arises because of the interaction between bosons and might disappear if the interaction becomes weaker. In Fig. 2(b) where $g_{1D} = 0.005$, the running-phase mode disappears and the π-mode MQST is surrounded by large closed circles referred as the π-mode Josephson oscillation. In Fig. 2(c) where $g_{1D} = 0.001$, the π-mode MQST disappears also.

$\Delta\theta$ is the conjugate variable of Δn. We can calculate the average phase in each well according to Eqs. (8) and (9). Fig. 3 shows θ_L, θ_R and $\Delta\theta$ for a Josephson oscillation case. It is worth noting that the phase of the condensate in each well varies much faster than the phase difference between the two wells. The phase in each well changes almost synchronously with slightly different high frequencies. In the two-mode model, θ_L and θ_R are not defined.

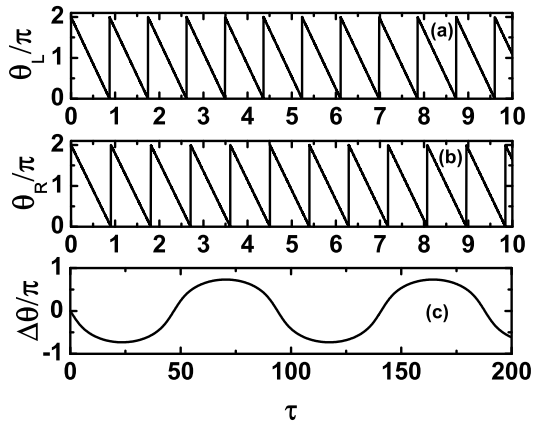

FIG. 3: Average phases in the left well, θ_L (a), the right well, θ_R (b) as well as the phase difference $\Delta\theta$ (c) for a Josephson oscillation case corresponding to the long-dashed line in Fig. 1a.

IV. THE DISSIPATION EFFECT

To proceed, we investigate dynamical behaviors of the double-well condensate subject to unavoidable dissipation. We consider a system described by phase space diagram in Fig. 2(a) and suppose that it is initially in a π-mode MQST state, ($\Delta n = 0.9$, $\Delta\theta = \pi$).

Fig. 4 shows the evolution trajectories calculated using Eq. (4). The dissipation parameter is chosen to be $\gamma = 0.01$, 0.03 and 0.1, respectively. In all the three cases, the trajectory passes through three different regimes. In the π-mode MQST regime, the system moves along an outward spiral path. Then it enters the running-phase MQST regime where the phase difference changes significantly. At last, it slides into the Josephson oscillation regime, along an inner spiral path. As discussed above, the energy decreases from the π-mode MQST to the Josephson oscillation. Therefore such trajectories imply that energy dissipates gradually. Moreover, the larger the dissipation parameter is, the faster the system drops into the lowest energy state.

Marino *et al.* have extended the two-mode model to include the dissipation effect [32]. The dissipation term they employed is based on the address in Ref. [3], where it was assumed to be an Ohmic current of normal atoms which causes energy dissipation. Present study is qualitatively consistent with results of Ref. [32]. Since our approach is an extension of the TDGP equation approach, we believe that the obtained results provide a more quantitatively accurate description of the dissipation process for the double-well condensate and are expected to be compared with experiments, as discussed in Sect. III.

To illustrate the dissipation process clearly, we calcu-

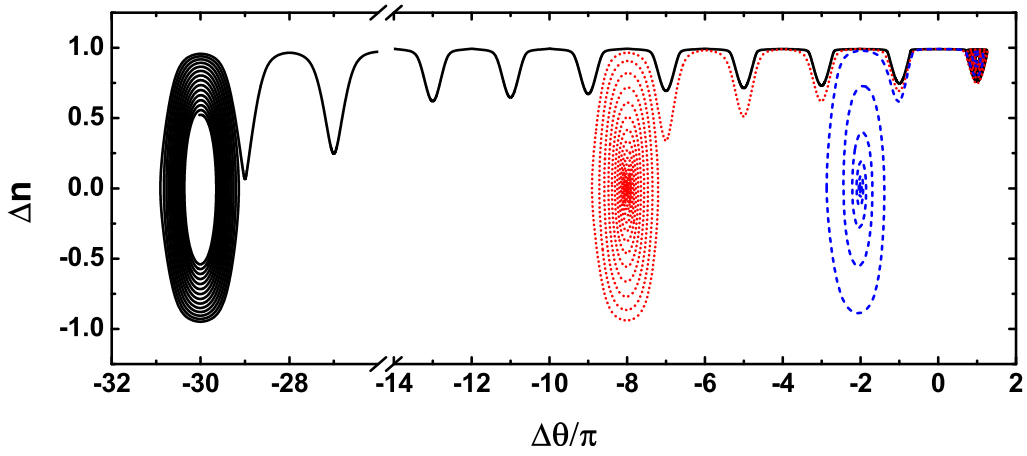

FIG. 4: (Color online) Evolution trajectories of a system initially in the π-mode MQST state ($\Delta n = 0.9$, $\Delta\theta = \pi$) with different dissipation parameters, $\gamma = 0.01$ (solid line), $\gamma = 0.03$ (short-dotted line), and $\gamma = 0.1$ (short-dashed line), respectively.

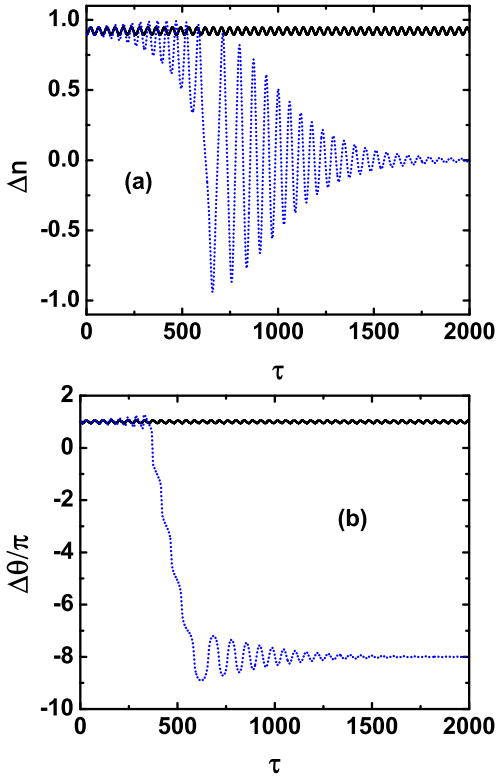

FIG. 5: (Color online) Evolution of Δn (a) and $\Delta\theta$ (b) starting from a π-mode MQST point ($\Delta n = 0.9$, $\Delta\theta = \pi$) with dissipation parameters $\gamma = 0.03$ (short-dotted lines), compared with case without dissipation (solid lines).

abruptly from π to -8π, which is the typical character of the running-phase MQST regime. When $\Delta\theta$ starts to oscillate around -8π, the system enters into the Josephson oscillation regime. During this stage, both Δn and $\Delta\theta$ oscillate in a sine-like way, but their amplitudes damp with time. Finally, Δn arrives at the value of zero which represents an equilibrium distribution of particles in the two wells.

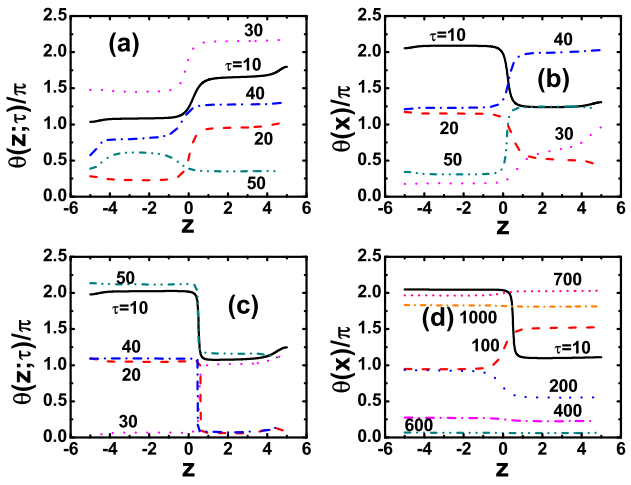

FIG. 6: (Color online) Snapshots of phase distributions in the double-well at different given times. (a), (b) and (c) depict the Josephson oscillation, running-phase MQST and π-mode MQST cases without dissipation, respectively. (d) shows the dissipation prosess from the π-mode MQST state with $\gamma = 0.03$.

late time-evolutions of the population imbalance and the phase difference, taking the $\gamma = 0.03$ case as an example, as shown in Fig. 5. When τ is less than 350, the system is still in the π-mode MQST regime where both Δn and $\Delta\theta$ oscillate around the center of the π-mode MQST region, although their amplitudes grow slightly. During the interval from $\tau \sim 350$ to $\tau \sim 600$, $\Delta\theta$ drops

An advantage of the TDGP equation approach is that it provides spatial information of the phase distribution in each well [22]. Fig. 6 illustrates the phase distribution, $\theta(z;\tau)$, for different dynamical processes. In all the cases, the phase keeps almost a constant in each well, except at the edges of the well. Even if the phase varies with the position, the deviation is usually very small. This accounts

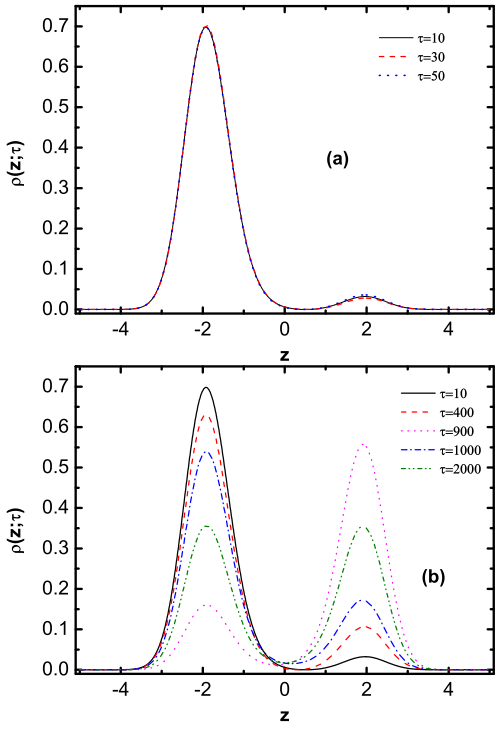

FIG. 7: (Color online) Snapshots of particle density distributions in the double-well. (a) depicts the π-mode MQST case without dissipation. (b) shows the dissipation prosess from the π-mode MQST state with $\gamma = 0.03$.

for the validity of the use of two-mode approximation. An interesting observation is that the phase distribution in the well with more particles seems flatter than that in the well with less particles. This point is demonstrated in Fig. 6(b) and 6(c) which depict the MQST cases with the left well trapping more particles. We also find that the phase distribution in the dissipative case is much flatter, as if the dissipation tends to suppress phase fluctuation in each well, as shown in Fig. 6(d).

Fig. 6 also shows that the phase $\theta(z;\tau)$ may change abruptly near the barrier, but not right at $z = 0$. Taking Fig. 6(c) which describes the π-mode MQST as an example, there is an insanely steep gradient near $z \approx 0.5$ on each lines.

We now look at the particle density distribution. Fig. 7(a) displays the π-mode MQST case without dissipation, where $n(z)$ exhibits two peaks located in the two wells respectively. Obviously, the left peak keeps higher than the right one all the time. We note that the minimum between the two peaks does not lie at the center of the barrier. It is biased towards the right side of the barrier. This accounts for the reason why $\theta(z;\tau)$ begins to change abruptly on right side of the barrier. We judge that the abrupt change in $\theta(z;\tau)$ takes place at the minimum point of the particle density distribution between the two density peaks. Fig. 7(b) shows the dissipation process from the π-mode MQST with $\gamma = 0.03$. Then the system evolves into the running-phase MQST regime (see the $\tau = 400$ line) and the Josephson oscillation regime (see $\tau = 900$, 1000 and 2000 lines). At $\tau = 2000$, the system becomes almost stable.

V. CONCLUSION

In conclusion, we have investigated dynamic properties of the double-well Bose-Einstein condensate subject to dissipation in the framework of time-dependent Gross-Pitaevskii equation. The phase space diagram for the system without dissipation are systematically produced and three typical dynamical regimes of Josephson oscillation, π-mode MQST and running phase MQST are shown clearly. The energy dissipation processes are studied by introducing a phenomenological dissipation term to the TDGP equation. The evolution trajectories evolve gradually from the high energy states to the low energy states, suggesting that this approach is applicable to describing energy dissipation effect. Relevant results have been studied previously based on two-mode model. We expect that the TDGP approach provides a more quantitatively accurate description of the dissipation process for the double-well condensate and the results are expected to be compared with experiments.

Moreover, the TDGP approach produces spatial information of the phase distribution and density profile which are not directly reflected in two-mode model calculations. The phase of condensate varies slowly in space in each well and may exhibit abrupt changes near the barrier, but not certainly at the barrier center. These sudden changes occur at the minimum position in particle density profile. We also note that the average phase in each well varies much faster with time than the phase difference between two wells.

Acknowledgments

This work is supported by the National Natural Science Foundation of China (Grant No. 11074021 and Grant No. 11004007), and the Fundamental Research Funds for the Central Universities of China.

[1] J. Javanainen, Phys. Rev. Lett. **57**, 3164 (1986).
[2] M. W. Jack, M. J. Collett and D. F. Walls, Phys. Rev. A **54**, R4625 (1996).
[3] I. Zapata, F. Sols and A. J. Leggett, Phys. Rev. A **57**, R28 (1998).
[4] A. Smerzi, S. Fantoni, S. Giovanazzi and S. R. Shenoy,

Phys. Rev. Lett. **79**, 4950 (1997).
[5] S. Raghavan, A. Smerzi, S. Fantoni and S. R. Shenoy, Phys. Rev. A **59**, 620 (1999); S. Giovanazzi, A. Smerzi, and S. Fantoni, Phys. Rev. Lett. **84**, 4521 (2000).
[6] G. J. Milburn, J. Corney, E. M. Wright and D. F. Walls, Phys. Rev. A **55**, 4318 (1997).
[7] M. J. Steel and M. J. Collett, Phys. Rev. A **57**, 2920 (1998).
[8] A. Vardi and J. R. Anglin, Phys. Rev. Lett. **86**, 568 (2001). J. R. Anglin and A. Vardi, Phys. Rev. A **64**, 013605 (2001).
[9] K. Sakmann, A. I. Streltsov, O. E. Alon, and L. S. Cederbaum, Phys. Rev. Lett. **103**, 220601 (2009).
[10] M. Trujillo-Martinez, A. Posazhennikova and J. Kroha, Phys. Rev. Lett. **103**, 105302 (2009).
[11] E. Boukobza, M. Chuchem, D. Cohen, and A. Vardi, Phys. Rev. Lett **102**, 180403 (2009). E. Boukobza, D. Cohen and A. Vardi, Phys. Rev. A **80**, 053619 (2009).
[12] B. Juliá-Díaz, D. Dagnino, M. Lewenstein, J. Martorell, and A. Polls, Phys. Rev. A **81**, 023615 (2010); B. Juliá-Díaz, J. Martorell, M. Melé-Messeguer and A. Polls, Phys. Rev. A **82**, 063626 (2010).
[13] J. Ruostekoski and D. F. Walls, Phys. Rev. A **58**, R50 (1998).
[14] I. Zapata, F. Sols and A. J. Leggett, Phys. Rev. A **67**, 021603 (2003).
[15] D. Witthaut, F. Trimborn and S. Wimberger, Phys. Rev. Lett. **101**, 200402 (2008); Phys. Rev. A **79**, 033621 (2009).
[16] S. Diehl, A. Micheli, A. Kantian, B. Kraus, H. P. Büchler and P. Zoller, Nature. Phys. **4**, 878 (2008).
[17] M. R. Andrews, C. G. Townsend, H.-J. Miesner, D. S. Durfee, D. M. Kurn and W. Ketterle, Science **275**, 637 (1997).
[18] M. Albiez, R. Gati, J. Fölling, S. Hunsmann, M. Cristiani and M. K. Oberthaler, Phys. Rev. Lett. **95**, 010402 (2005).
[19] R. Gati and M. K. Oberthaler, J. Phys. B: At. Mol. Opt. Phys. **40**, R61 (2007).
[20] S. Levy, E. Lahoud, I. Shomroni and J. Steinhauer, Nature **449**, 579 (2007).
[21] T. Zibold, E. Nicklas, C. Gross and M. K. Oberthaler, Phys. Rev. Lett. **105**, 204101 (2010).
[22] D. Ananikian, and T. Bergeman, Phys. Rev. A **73**, 013604 (2006).
[23] M. Melé-Messeguer, B. Juliá-Díaz, M. Guilleumas, A. Polls and A. Sanpera, New J. Phys. **13** 033012 (2011).
[24] Y. Cai, M. Rosenkranz, Z. Lei and W. Bao, Phys. Rev. A **82**, 043623 (2010).
[25] P. Muruganandam and S. K. Adhikari, Comput. Phys. Commun. **180**, 1888 (2009).
[26] S. Choi, S. A. Morgan and K. Burnett, Phys. Rev. A **57**, 4057 (1998).
[27] E. Zaremba, T. Nikuni and A. Griffin, J. Low Temp. Phys. **116**, 277 (1999).
[28] M. Tsubota, K. Kasamatsu and M. Ueda, Phys. Rev. A **65**, 023603 (2002); K. Kasamatsu, M. Tsubota and M. Ueda, Phys. Rev. A **67**, 033610 (2003);
[29] H. Saito and M. Ueda, Phys. Rev. A **70**, 053610 (2004).
[30] L. Wen, H. Xiong and B. Wu, Phys. Rev. A **82**, 053627 (2010).
[31] S. P. Cockburn, H. E. Nistazakis, T. P. Horikis, P. G. Kevrekidis, N. P. Proukakis, and D. J. Frantzeskakis, Phys. Rev. A **84**, 043640 (2011).
[32] I. Marino, S. Raghavan, S. Fantoni, S. R. Shenoy and A. Smerzi, Phys. Rev. A **60**, 487 (1999).